1990

Hydrodynamic models for the RRc stars

Norman R. Simon
University of Nebraska - Lincoln, nsimon@unl.edu

Mon. Not. R. astr. Soc. (1990) **246,** 70–77

Hydrodynamic models for the RRc stars

Norman R. Simon

Department of Physics and Astronomy, University of Nebraska–Lincoln, Lincoln, NE 68588-0111, USA

Accepted 1990 March 20. Received 1990 March 7; in original form 1989 September 19

SUMMARY

Hydrodynamic pulsation models are constructed for the RR Lyrae stars, including a large grid of RRc models and a pair of models with parameters corresponding to the RRd stars. The latter calculations are used to argue that LNA periods are sufficient when comparing RRd models with observations. The RRc models are subjected to Fourier decomposition, and a discussion of various Fourier parameters is undertaken to complement a treatment given elsewhere of the phase parameter ϕ_{31}. It is shown that the theoretical light curves mimic the observations rather well, including the observed run of ϕ_{31} with period and the fall-off of ϕ_{31} with R_{21}. The greatest deficiency of the models lies in their failure to reproduce observed values of the phase parameter ϕ_{21}. Finally, turning to the velocity curves, we show that the first-order phase lag $(\Delta\phi)_1$ between velocity and light is related in the models to the linear driving η_1 and thus potentially may be used to measure the distances of observed RRc stars from their respective blue edges.

1 INTRODUCTION

The RR Lyrae pulsators have a long-standing role in a number of crucial astronomical problems including horizontal branch evolution, galactic structure and history, and the cosmic distance scale. These stars divide naturally into three groups: the fundamental-mode pulsators (RRab stars), the first-overtone pulsators (RRc stars), and finally, the objects which pulsate simultaneously in both modes (RRd stars). The RR Lyrae stars have been much studied. In the last two decades, hydrodynamic pulsation models have been constructed for these objects with varying degrees of success in reproducing their observed properties. Recent RR Lyrae models include those by Stothers (1981), Simon & Aikawa (1986), Hubickyj & Stothers (1986) and Kovacs & Buchler (1988).

Simon (1985) used Fourier decomposition to compare the Strothers and Hubickyj–Stothers models with observations. In this technique (Simon 1988a, and references therein), the observed and theoretical light curves are fitted with Fourier series, namely,

$$\text{mag} = A_0 + A_j \cos(j\omega t + \phi_j) \quad (\text{sum over } j), \tag{1}$$

and then compared in terms of combinations of the low-order coefficients:

$$R_{j1} = A_j/A_1,\ \phi_{j1} = \phi_j - j\phi_1. \tag{2}$$

Although the sample of models was small, Simon (1985) found that the first-overtone calculations were much more successful in modelling the RRc stars, than were the fundamental-mode models in mimicking the RRab stars.

It was this result that prompted the calculation of the large grid of first-overtone models whose properties will be described below. A number of results obtained from the study of these calculations have already been given by Simon (1989, hereafter S89). The models were found to be particularly successful in reproducing the observed Fourier phase parameter ϕ_{31}. It was shown in S89 that this parameter measures the luminosity-to-mass ratio $L/M^{1.81}$ for the RRc stars. Comparison of the models with observed light curves of RRc pulsators in the globular cluster ω Centauri led S89 to conclude that the masses of the RRc stars in ω Cen agree with the masses determined for a sample of RRd stars in other clusters (see below; also Cox 1988). Some of these conclusions are implicit already in Hubickyj & Stothers (1986) who, based upon qualitative and semi-quantitative arguments, derived RRc masses in the range 0.55–0.65 $M_\odot$ and emphasized the importance of the luminosity-to-mass ratio in determining light-curve properties.

The present hydrodynamic models were constructed with the dynamically zoned code TGRID, described by Aikawa & Simon (1983) and Simon & Aikawa (1986). The opacities were in the form of an analytic fit given by Stellingwerf (1975). Convection was neglected. The main body of the current work will be devoted to discussing the properties of 42 first overtone models which comprise the bulk of our calculations. This discussion begins in Section 3. However, before proceeding with this subject, we shall briefly treat in,

Section 2, a small group of additional models designed to study the RRd stars.

2 RRd MODELS

The RRd stars pulsate simultaneously in the first-overtone and fundamental modes. A recent discussion of these objects was given by Cox (1988). It was argued by Cox, Hodson & Clancy (1983) that the RRd variables are located in the instability strip near the boundary separating the regions occupied by the RRc (first-overtone) and RRab (fundamental mode) pulsators. Furthermore, when these authors plotted the RRd periods on the Petersen diagram (period ratio versus period), it was found that the stars separated clearly into two groups – corresponding to Oosterhoff I (Oo I) and Oosterhoff II (Oo II) clusters, respectively [see Rood & Crocker (1989) for a description of the Oosterhoff groups]. Finally, linear non-adiabatic (LNA) pulsation models were employed to deduce masses for the RRd stars, with the result as follows: Oo I clusters: $M \approx 0.55\ M_{\odot}$; Oo II clusters: $M \approx 0.65\ M_{\odot}$ (Cox *et al.* 1983).

The RRd period ratios are observed with extremely high accuracy, of the order 0.001 (e.g. Clement *et al.* 1986). Since the difference between the Oo I and Oo II RRd stars is found to be $\delta(P_1/P_0) \leqq 0.002$, it is crucial for the mass determinations that the theoretical periods are highly reliable. One possible source of error lies in the fact that *linear* models were used to find the periods, whereas it is clear that only models at limiting amplitude are appropriate for comparison with observations. Because it is a very time-consuming process to integrate hydrodynamic models until they approach limiting amplitude, it was decided to test the linear periods in two cases only, corresponding to the Oo I and Oo II groups, respectively.

Table 1 displays parameters for the two models we chose. The LNA periods and growth rates (per cent per period) are given for the fundamental and first-overtone models in each model. These periods place Model A among the Oo I stars in the Petersen diagram, and Model B among the Oo II stars. Each model was perturbed in the fundamental mode and integrated for many periods until approximate convergence. The calculation was then repeated for a first-overtone perturbation. The fourth and seventh columns of Table 1 give integration times τ_0 and τ_1 (in periods) for the fundamental and overtone calculations, respectively.

Fig. 1 portrays the last few hundred periods for the *F*-mode integration in Model B. The abscissa is time and the top ordinate the maximum kinetic energy attained (over the previous 10-period interval), both in arbitrary units. One notes that the kinetic energy has converged to about one part in 10^3. The bottom panel shows the pulsation frequency (arbitrary units) determined at the indicated times via a 'maximum entropy' analysis (Ulrich & Bishop 1975; Uji-iye 1986) performed on data spanning in each case the previous 100 pulsation periods. The dashed line indicates the frequency emerging from the LNA calculation. Noting the narrow range of the frequency scale (fourth significant figure) one remarks on the close agreement of the limiting and LNA frequencies.

In Fig. 2 we show a similar plot for the first-overtone mode of Model B. Again the kinetic energy has converged very tightly and the non-linear frequency is very close to the linear value. Averaging the frequencies in Figs 1 and 2, we obtain $f_0 = 2.1146$, $f_1 = 2.8319$ and thus $f_0/f_1 = P_1/P_0 = 0.7467$, in close agreement with the LNA period ratio given in Table 1.

Table 1. Parameters of RRd models.

	$\frac{M}{M_{\odot}}$	$\log\frac{L}{L_{\odot}}$	T_e	Y	Z	$\frac{P_1}{P_0}$
Model A	0.55	1.660	7000	0.250	0.001	0.7449
Model B	0.67	1.780	6950	0.250	0.0002	0.7464

	P_0	η_0 (x10^3)	τ_0 (per)	P_1	η_1 (x10^3)	τ_1 (per)
Model A	0.48384	3.85	1300	0.36040	17.8	2510
Model B	0.54731	3.05	1210	0.40851	18.1	1730

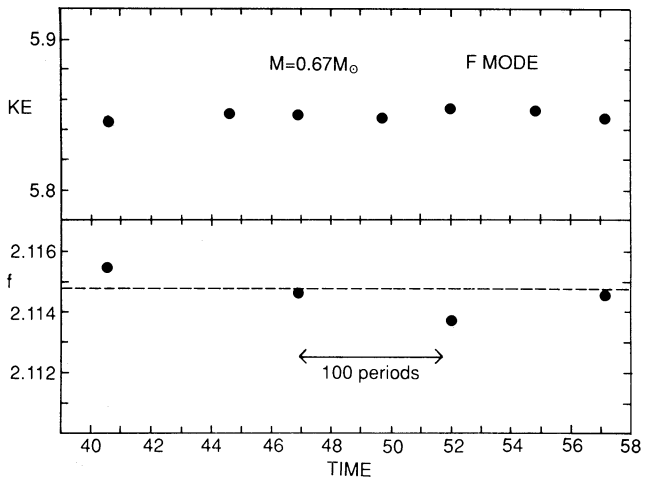

Figure 1. Kinetic energy and pulsation frequency versus time (all in arbitrary units) for the last few hundred periods of the fundamental-mode integration in Model B. The dashed line indicates the LNA frequency.

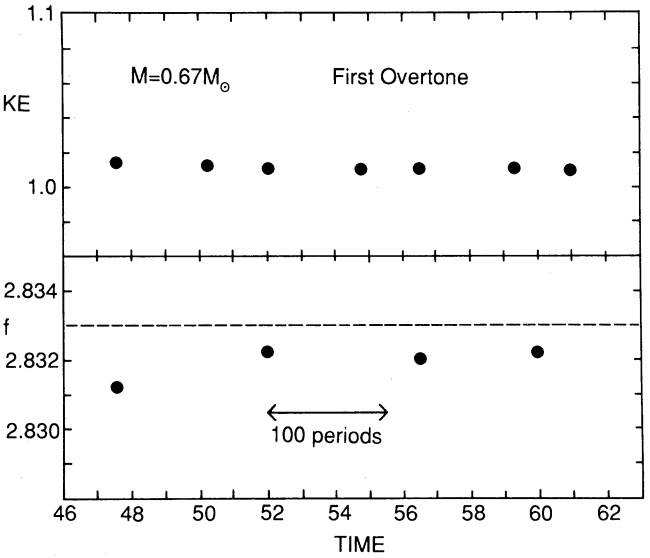

Figure 2. Same as Fig. 1, but for the first-overtone mode in Model B.

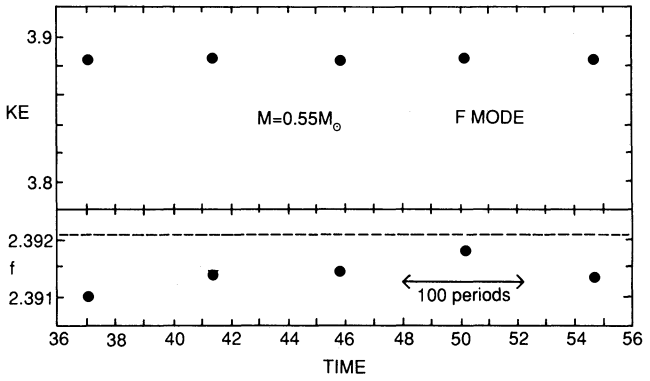

Figure 3. Same as Fig. 1, but for the fundamental mode in Model A.

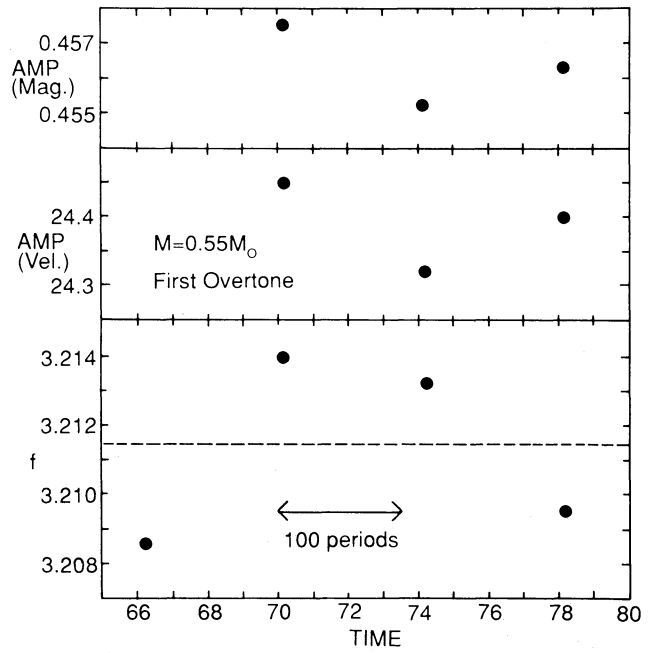

Figure 4. Magnitude and velocity amplitudes along with frequency for the first-overtone integration in Model A. The dashed line indicates the LNA frequency.

Fig. 3 displays the time evolution of the fundamental mode in Model A. Once more we see that the model has converged and that the limiting frequency agrees with the LNA value to one part in 10^3. The first-overtone integration for Model A was somewhat more problematical. In this case, a very small F-mode component remained in the oscillation even after 2500 periods. Unfortunately, the kinetic energy record for the last few hundred periods was lost; however, the light and velocity amplitudes were retained and these are shown plotted against time in the top two panels of Fig. 4. These amplitudes were steady to within about 0.002 mag and 0.2 km s^{-1}, respectively. Furthermore, Fourier decompositions of the light and velocity curves showed that the coefficients were also very steady over the time range in question. There was no reason to believe that the very small fundamental-mode contribution was anything but a slowly fading transient. Indeed, this conclusion is strongly bolstered by the results of Kovacs & Buchler (1988) who, using a relaxation (as opposed to initial-value) technique, found no evidence for instability of the first-overtone limit cycle in models with parameters very close to those of our Model A.

The bottom panel of Fig. 4 shows the overtone frequency as a function of time in Model A for the last few hundred periods. The values are seen to scatter about the LNA frequency. This scatter is larger than that in the other integrations, probably due to the F-mode transient. Taking a simple time average in Figs 3 and 4 we find for Model A: $f_0 = 2.3914$, $f_1 = 3.2113$, $P_1/P_0 = 0.7447$. The latter number is again in close agreement with the LNA value given in Table 1.

Because we are dealing with non-linear systems it cannot be ruled out that the agreement between the linear and non-linear periods in Models A and B is fortuitous and thus subject to change over longer time periods. However, the present calculations taken in concert with similar results obtained by Kovacs & Buchler (1988) for a series of relaxation models and a single initial-value integration strongly suggest that LNA periods are sufficient for comparison with the observed periods of the RRd stars.

3 RRc MODELS

The main body of calculations consisted of 42 models with parameters in the range: $0.50 \leqq M/M_\odot \leqq 0.70$, $1.54 \leqq \log L/L_\odot \leqq 1.86$, $6850 \leqq T_e \leqq 7500$ K. The metal abundance was $Z = 0.001$ for $M < 0.65\,M_\odot$, and $Z = 0.0002$ for $M \geqq 0.65\,M_\odot$. The helium abundance was taken to be either $Y = 0.25$ or $Y = 0.30$. For given M, L and Y, two models were calculated – one near the first-overtone bulge edge and another near or just redward (< 100 K) of the fundamental-mode blue edge. This spans the domain in which most RRc stars are likely to be found. Table 2 lists the model parameters, including the LNA periods and the linear growth rate ($\times 10^3$) of the first overtone (η_1). The fundamental mode is linearly stable in all models except as indicated by a footnote in the η_1 column.

The hydrodynamic models were perturbed with a velocity distribution dominated by the LNA eigenfunction corresponding to the first overtone. Integrations were then continued for a time interval between 100 and 200 periods. This was sufficient for the light and velocity curves to settle down close to their limiting forms. In particular, the crucial Fourier parameter ϕ_{31} was found to change, typically, by 0.1 or less over the last 30–60 periods of the oscillation. The artificial viscosity parameters (Stellingwerf 1975) in all of the Table 2 models were set at $C_Q = 2.0$, $\alpha = 0.01$.

Simon & Aikawa (1986) have published a number of light and velocity curves calculated with the TGRID code. These curves tend to be very smooth, owing to TGRID's dynamic zoning in the hydrogen-ionization region. Fig. 5 displays the raw output emerging from one of our present well-converged calculations, Model 65N (see Table 2). The top curve shows the velocity (km s^{-1}) in theoretician's units (expansion phase positive) while the lower curve gives the luminosity (arbitrary units). Along the abscissa, the time is also plotted in arbitrary units. Once more, the smooth curves are typical of RR Lyrae models constructed with TGRID.

Table 2. Parameters of RRc models.

Model	$\log\frac{L}{L_\odot}$	T_e	Y	P_1	$\frac{P_1}{P_0}$	η_1 ($\times 10^3$)
			M = 0.50 $M_\odot$			
50A	1.54	7300	.250	.266	.750	1.65
50B	1.54	7000	.250	.306	.747	23.0*
50C	1.54	7500	.300	.243	.752	2.04
50D	1.66	7350	.300	.324	.745	1.55
			M = 0.55 $M_\odot$			
55A	1.54	7300	.250	.251	.754	4.28
55B	1.56	7300	.250	.261	.753	3.01
55C	1.58	7200	.250	.283	.751	7.74
55D	1.58	7050	.250	.303	.749	18.5*
55E	1.58	7450	.300	.253	.753	4.14
55F	1.58	7200	.300	.283	.751	19.5*
55G	1.66	7200	.250	.328	.747	0.24
55H	1.66	7000	.250	.360	.745	17.8*
55I	1.66	7400	.300	.299	.749	1.48
55J	1.66	7200	.300	.328	.747	17.3
55K	1.70	7100	.250	.371	.744	3.25
55L	1.70	6950	.250	.398	.742	18.1*
55M	1.70	7350	.300	.329	.746	1.25
55N	1.74	7050	.250	.409	.742	3.05
55P	1.74	6900	.250	.439	.740	17.5*
55Q	1.74	7250	.300	.372	.744	5.33
55R	1.74	7050	.300	.408	.742	25.7*
			M = 0.65 $M_\odot$			
65A	1.66	7250	.250	.291	.755	3.10
65B	1.70	7200	.250	.319	.752	3.40
65C	1.70	7050	.250	.343	.750	14.6*
65D	1.70	7400	.300	.291	.754	2.42
65E	1.70	7200	.300	.319	.752	15.2
65F	1.74	7150	.250	.352	.750	3.40
65G	1.78	7100	.250	.388	.747	3.25
65H	1.78	6950	.250	.416	.745	17.3*
65I	1.78	7300	.300	.353	.749	3.48
65J	1.78	7100	.300	.387	.747	21.0*
65K	1.82	7050	.250	.427	.745	3.75
65L	1.82	6900	.250	.459	.743	17.8*
65M	1.82	7250	.300	.389	.746	3.57
65N	1.86	7000	.250	.472	.742	2.31
65O	1.86	6850	.250	.508	.740	17.6*
65P	1.86	7200	.300	.430	.744	3.12
65Q	1.86	7000	.300	.471	.742	24.7*
			M = 0.70 $M_\odot$			
70A	1.70	7200	.250	.306	.756	4.76
70B	1.70	7000	.250	.335	.753	17.3*
70C	1.82	7100	.250	.400	.748	2.47
70D	1.82	6900	.250	.439	.746	20.3*

*F mode also unstable.

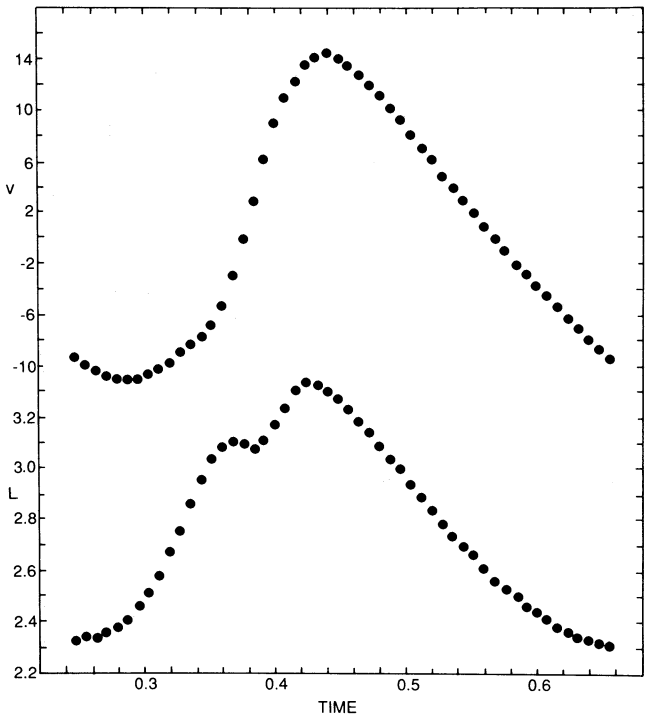

Figure 5. Velocity (km s^{-1}, expansion phase positive) and luminosity (arbitrary units) versus time (arbitrary units) for Model 65N.

4 FOURIER DECOMPOSITIONS

For the purposes of analysis we converted the surface luminosities in all 42 models into bolometric magnitudes, and multiplied the velocities by the well-known factor −17/24 to convert them to 'observational' form (expansion phase negative). Eighth-order Fourier decompositions were then performed on the converted light curves according to the form given in equation (1) and on the velocity curves according to the form

$$v = A_0 - A_j \sin(j\omega t + \phi_j) \quad (\text{sum over } j). \tag{3}$$

Standard deviations for the Fourier fits were typically ~0.02 mag for the light curves and <1 km s^{-1} for the velocities.

Results from the Fourier analysis of the light curves are given in Table 3, which includes a number of models not appearing in Table 2. First, the Fourier parameters for the overtone pulsations of Models A and B of Section 2 are given in Table 3 as Models 55H and 67A, respectively. And secondly, Table 3 includes three models with the suffix '1'; these have model parameters identical to those of Models 55N, 65B and 55H, respectively, but were calculated with smaller artificial viscosity – namely, $C_Q = 1.0$, $\alpha = 0.01$. In the columns of Table 3 we list limiting amplitudes for the light curves as well as the first four Fourier amplitude ratios and phase differences as defined in equations (2).

The corresponding quantities for the velocity curves (see equations 2 and 3) are displayed in Table 4. The final column of Table 4 gives the first-order phase lag between maximum light and maximum expansion velocity (Simon 1984) with the definition

$$(\Delta\phi)_1 = \phi_1(\text{velocity}) - \phi_1(\text{light}) + \pi/2.$$

Table 3. Fourier decompositions for model light curves.

Model	AMP (mag)	R_{21}	ϕ_{21}	R_{31}	ϕ_{31}	R_{41}	ϕ_{41}
50A	.38	.171	4.57	.0379	3.40	.0259	1.10
50B	.54	.211	4.70	.120	3.14	.101	1.76
50C	.32	.164	4.46	.0245	3.64	.0140	1.07
50D	.33	.0757	4.84	.0328	4.44	.0253	2.30
55A	.45	.254	4.31	.0438	3.06	.0317	.698
55B	.43	.233	4.39	.0408	3.24	.0289	.656
55C	.48	.244	4.51	.0576	2.87	.0432	1.15
55D	.56	.264	4.61	.110	2.75	.0772	1.27
55E	.39	.213	4.31	.0334	3.43	.0173	.650
55F	.57	.286	4.54	.0872	2.86	.0541	1.55
55G	.35	.130	4.74	.0424	3.61	.0282	1.50
55H	.46	.171	4.65	.106	3.50	.0989	2.05
55H1	.56	.170	4.65	.128	3.45	.129	2.04
55I	.33	.138	4.68	.0220	3.82	.0155	1.51
55J	.49	.187	4.75	.0666	3.31	.0636	1.94
55K	.41	.113	4.67	.0785	4.06	.0637	2.18
55L	.49	.135	4.75	.0676	4.00	.0750	2.57
55M	.31	.0987	4.87	.0273	4.29	.0141	2.10
55N	.40	.0893	4.66	.0463	4.63	.0466	2.72
55N1	.47	.101	4.78	.0457	4.40	.0551	2.70
55P	.47	.0936	4.53	.0408	4.02	.0525	2.68
55Q	.38	.0727	4.80	.0319	4.67	.0310	2.50
55R	.49	.0923	4.91	.0480	4.17	.0663	2.68
65A	.46	.255	4.28	.0440	3.16	.0295	.561
65B	.45	.240	4.44	.0396	2.99	.0347	.933
65B1	.51	.268	4.48	.0583	2.63	.0442	.972
65C	.54	.274	4.51	.0853	2.67	.0542	1.13
65D	.38	.205	4.27	.0335	3.15	.0138	.624
65E	.57	.308	4.42	.0715	2.73	.0386	1.36
65F	.43	.197	4.58	.0448	3.10	.0383	1.23
65G	.42	.159	4.70	.0560	3.35	.0457	1.48
65H	.51	.182	4.60	.109	3.33	.0975	1.91
65I	.39	.162	4.65	.0188	4.02	.0240	1.33
65J	.52	.199	4.72	.0771	3.22	.0708	1.92
65K	.41	.116	4.62	.0788	3.87	.0677	2.07
65L	.50	.150	4.68	.0731	3.90	.0787	2.52
65M	.37	.126	4.75	.0243	4.27	.0257	1.78
65N	.42	.0993	4.66	.0528	4.62	.0525	2.72
65O	.49	.103	4.57	.0406	4.03	.0530	2.71
65P	.36	.0856	4.80	.0323	4.52	.0291	2.32
65Q	.50	.103	4.77	.0514	4.09	.0712	2.69
67A	.50	.201	4.61	.119	3.09	.0976	1.72
70A	.49	.273	4.22	.0407	2.85	.0304	.548
70B	.65	.358	4.36	.125	2.48	.0615	.807
70C	.41	.181	4.62	.0471	3.17	.0422	1.31
70D	.53	.208	4.59	.113	3.19	.0923	1.89

Table 4. Fourier decomposition for model velocity curves.

Model	AMP (vel)	R_{21}	ϕ_{21}	R_{31}	ϕ_{31}	R_{41}	ϕ_{41}	$(\Delta\phi)_1$
50A	15.8	.202	5.56	.0526	4.93	.0261	4.45	-.594
50B	28.4	.306	5.85	.100	5.45	.0469	4.80	-.471
50C	13.3	.156	5.43	.0473	4.70	.0212	4.34	-.603
50D	14.4	.224	5.73	.0668	5.24	.0281	4.99	-.641
55A	18.8	.192	5.57	.0568	4.90	.0293	4.16	-.531
55B	17.7	.190	5.53	.0577	4.87	.0326	4.18	-.559
55C	21.0	.232	5.64	.0680	5.08	.0371	4.38	-.506
55D	27.7	.291	5.74	.0996	5.34	.0448	4.65	-.393
55E	16.7	.168	5.44	.0578	4.62	.0284	4.11	-.554
55F	28.2	.287	5.66	.119	5.15	.0636	4.56	-.381
55G	15.2	.204	5.69	.0489	5.09	.0250	4.65	-.596
55H	24.3	.299	5.87	.0980	5.35	.0556	4.74	-.431
55H1	-	-	-	-	-	-	-	-
55I	13.9	.193	5.54	.0546	5.02	.0267	4.62	-.604
55J	24.5	.301	5.72	.116	5.23	.0652	4.73	-.456
55K	18.7	.241	5.83	.0709	5.07	.0404	4.67	-.565
55L	24.4	.291	5.97	.105	5.49	.0623	5.12	-.436
55M	13.3	.203	5.66	.0579	5.19	.0270	4.88	-.619
55N	18.6	.246	5.93	.0810	5.43	.0422	5.19	-.574
55N1	22.5	.288	5.92	.118	5.46	.0746	5.24	-.565
55P	-	-	-	-	-	-	-	-
55Q	-	-	-	-	-	-	-	-
55R	26.3	.322	5.92	.131	5.56	.0798	5.26	-.448
65A	18.4	.171	5.54	.0499	4.76	.0252	4.02	-.525
65B	18.7	.202	5.59	.0539	4.98	.0309	4.28	-.519
65B1	20.6	.224	5.54	.0724	4.84	.0419	4.22	-.520
65C	24.9	.260	5.71	.0824	5.26	.0375	4.50	-.414
65D	-	-	-	-	-	-	-	-
65E	26.2	.257	5.61	.103	5.00	.0573	4.31	-.412
65F	18.3	.216	5.65	.0528	5.08	.0286	4.49	-.526
65G	18.5	.231	5.70	.0570	5.08	.0305	4.55	-.536
65H	25.8	.295	5.84	.0879	5.27	.0467	4.55	-.412
65I	-	-	-	-	-	-	-	-
65J	26.4	.308	5.73	.119	5.26	.0656	4.70	-.407
65K	18.7	.244	5.81	.0651	5.04	.0369	4.55	-.545
65L	25.6	.294	5.96	.103	5.46	.0592	5.01	-.412
65M	16.2	.231	5.64	.0695	5.09	.0347	4.85	-.566
65N	18.9	.245	5.91	.0826	5.34	.0455	5.07	-.557
65O	25.5	.291	6.03	.103	5.63	.0558	5.38	-.419
65P	-	-	-	-	-	-	-	-
65Q	26.2	.321	5.91	.128	5.53	.0773	5.19	-.427
67A	26.1	.302	5.82	.0909	5.36	.0445	4.57	-.390
70A	-	-	-	-	-	-	-	-
70B	30.3	.281	5.72	.109	5.29	.0441	4.62	-.348
70C	17.9	.221	5.67	.0533	5.06	.0298	4.53	-.527
70D	27.4	.305	5.87	.0928	5.42	.0436	4.66	-.360

5 DISCUSSION

In S89 the Fourier phase parameter ϕ_{31} was singled out and shown to be a valuable diagnostic for interpreting the observations of RRc stars. The present work is devoted to the discussion of some of the other properties of the theoretical results. We turn first to the lower viscosity models 55N1, 65B1 and 55H1. Comparing these with 55N, 65B and 55H, respectively, one notes, as expected, higher amplitudes and larger values of R_{21} in the low-C_Q models (Simon & Aikawa 1986). The important parameter ϕ_{31} is somewhat smaller in the low-C_Q calculations, with $\langle\Delta\phi_{31}\rangle = 0.2$.

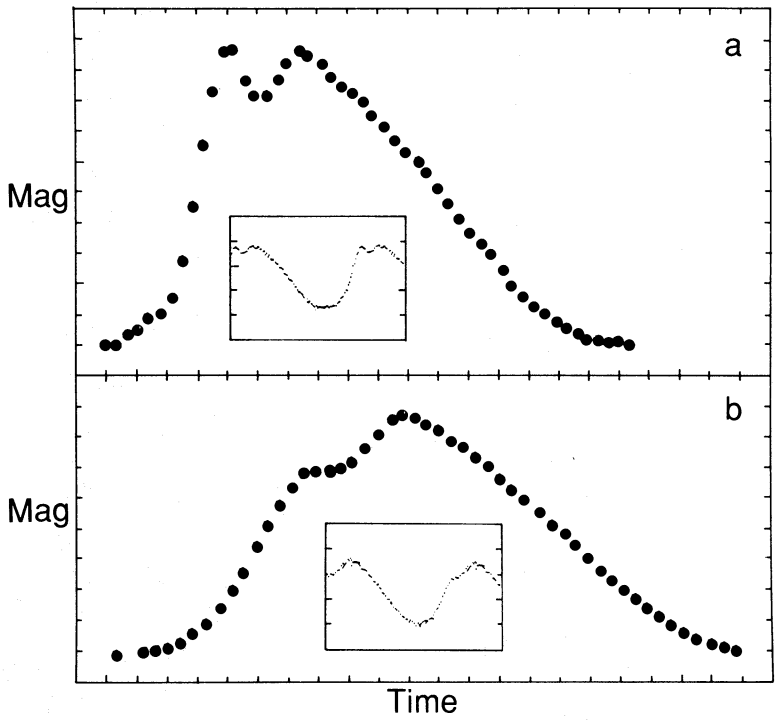

Figure 6. Theoretical and observed light curves for two cases: (a) Model 67A versus AU Vir (inset); (b) Model 65N versus V487 Sco (inset).

Although no strong dependence of Fourier parameters on artificial viscosity was found in this minimal experiment, a more comprehensive study (perhaps along the lines of Kovacs 1990) would certainly be in order.

Returning to the main body of calculations, one finds that the overall agreement between the hydrodynamic and observed RRc light curves is good. This agreement is illustrated in Fig. 6, where we display the light curves from two of the models (dots) along with two observed light curves from Lub (1977) (insets). In Fig. 6(a) the observed star is AU Vir ($P=0.343$d, $\phi_{31}=3.08$), while the model is 67A; Fig. 6(b) shows V487 Sco ($P=0.329$d, $\phi_{31}=4.47$) and Model 65N. These examples were chosen because they represent two extremes of light-curve shape seen in both the models and the

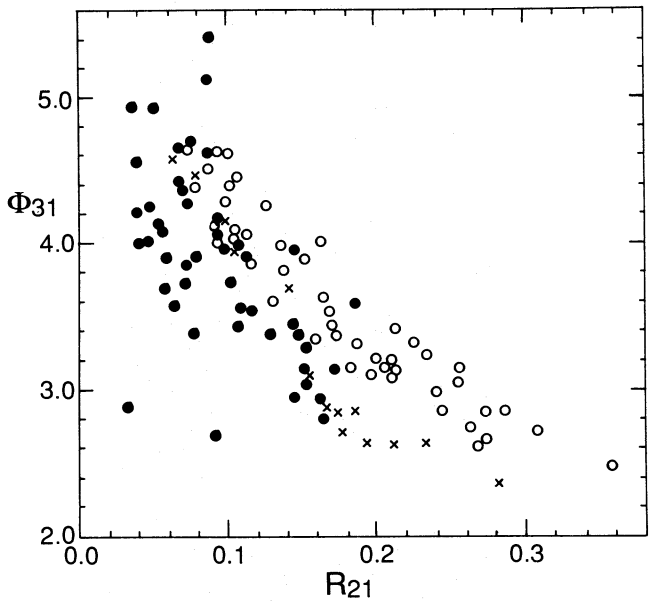

Figure 7. ϕ_{31} versus R_{21}. Dots: ω Cen RRc stars; crosses: field RRc stars; open circles: hydrodynamic models.

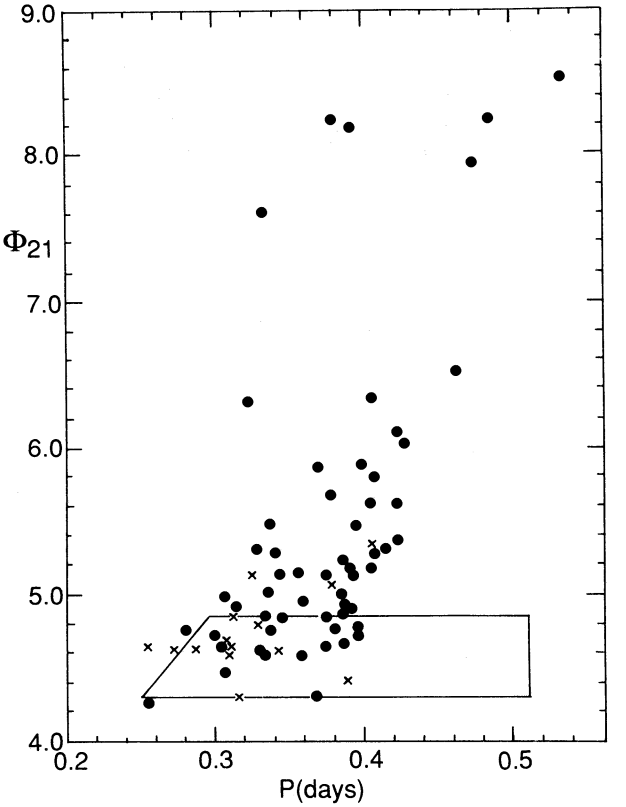

Figure 8. ϕ_{21} versus period. Dots: ω Cen RRc stars; crosses: field RRc stars. The box indicates the domain of the hydrodynamic models.

stars. The theoretical periods in these two cases are larger than the observed ones but this could be remedied, for example, by reducing the mass of the models while holding $\log(L/M^{1.81})$ fixed so as to fix ϕ_{31} (see S89). In any event, a completely satisfying agreement between theoretical and observed light-curve shapes is not yet to be expected since the models still have some faults. These shortcomings are better discussed in terms of the Fourier components, and this is the topic we address in what follows.

As seen in Fig. 6 the shape of the RRc light curves, particularly near maximum, seems crudely tied to the value of ϕ_{31}, with smaller ϕ_{31} yielding 'AU Vir type' curves and larger ϕ_{31}, 'V487 Sco types'. However, the situation is more complex, as illustrated in Fig. 7 where we plot ϕ_{31} versus the Fourier amplitude parameter R_{21}. The dots represent the 'reduced sample' of RRc stars from the globular cluster ω Cen (Petersen 1984; S89), and the crosses a sample of field RRc stars (Lub 1977; S89). We see a clear trend of falling ϕ_{31} with increasing R_{21}, so that these two Fourier parameters must operate in concert in defining the light-curve shapes. The hydrodynamic models (open circles) reproduce the observed trend but with values of R_{21} that are generally too high. This result is not surprising in view of the fact that R_{21} is somewhat amplitude-dependent (Simon & Lee 1981) whereas the hydrodynamic models do not give reliable limiting amplitudes (Simon 1988a). On balance, however, the ability of the models to show the observed fall-off in ϕ_{31} should be considered a positive factor.

A more serious problem concerns the Fourier phase parameter ϕ_{21}. Fig. 8 shows ϕ_{21} versus period for the reduced ω Cen sample (dots) and the field stars (crosses). Here, as with ϕ_{31}, there is a tendency to increase with period (see S89) but with considerably more scatter. The box drawn on the figure indicates the domain of the hydrodynamic models. It is clear that these models fail to reproduce the high values of ϕ_{21} attained by most of the stars. The quantity ϕ_{21} has long been the most problematic of the Fourier parameters in terms of

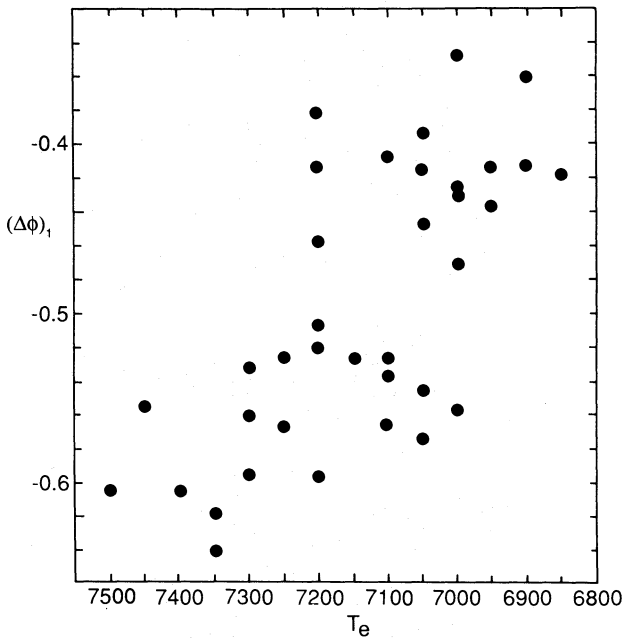

Figure 9. First-order phase lag $(\Delta\phi)_1$ versus T_e for the hydrodynamic models.

the ability of the theoretical models to match observed light curves (Simon 1988a). The models have a history of failing with ϕ_{21} even when succeeding with other parameters. It has been suggested by Simon (1988b) that the surface values of individual Fourier parameters are determined in critical interior zones which may be different for different parameters. In that case, the failure of models to reproduce observed values of a certain quantity (e.g. ϕ_{21}) would indicate physical or numerical shortcomings in the treatment of the interior domains critical in the determination of that quantity. In our opinion, the direct linking of Fourier para-

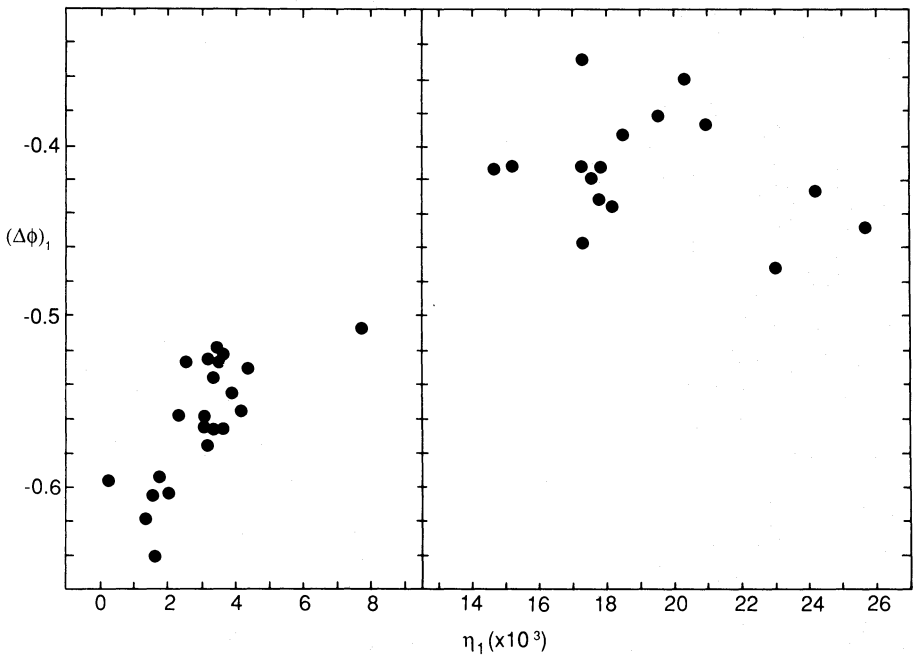

Figure 10. $(\Delta\phi)_1$ versus the linear driving η_1 in the theoretical models. The abscissa is compressed so as to omit the empty range, $9 \leqq \eta_1 \leqq 13$.

meters to the physical state of the envelope represents an important problem for future research.

Finally, let us turn to the calculated velocities. Detailed properties of the hydrodynamic velocity curves are made available in Table 4 but, with one exception, will not be treated further here due to the paucity of relevant observations. The exception concerns the first-order phase lag, $(\Delta\phi)_1$. Simon (1985) and Simon & Aikawa (1986) suggested that $(\Delta\phi)_1$ may serve as a temperature diagnostic and, indeed, a plot of $(\Delta\phi)_1$ versus T_e, shown here in Fig. 9, indicates such a relation, but with scatter large enough to make temperature determination very uncertain.

A more interesting relationship is shown in Fig. 10 where $(\Delta\phi)_1$ is plotted against the linear driving η_1. Because of the way we chose our models (see S89), they show small and large values of η_1 but few values in between. This circumstance is reflected in the compressed abscissa in Fig. 10 where we have entirely omitted the (empty) range, $9 \leqq \eta_1 \leqq 13$. It can be seen that at large η_1 the models attain less negative values of the phase lag, with considerable scatter. However, when the driving is small (say, $\eta_1 < 5$), there is a rather sharp increase of $(\Delta\phi)_1$ with η_1, with the models showing phase lags $\leqq -0.5$. If these results are correct (i.e. if the models prove reliable in reproducing observed phase lags), then Fig. 10 provides a method of measuring the distance of RRc stars from their respective blue edges, at least for those stars which are relatively hot (small driving). A test of this suggestion will require a set of RRc velocity curves, but since first-order Fourier quantities are involved in $(\Delta\phi)_1$, the demands on the velocity data may not be too onerous.

ACKNOWLEDGMENTS

The author is grateful to the University of Nebraska for a Maude Hammond Fling Fellowship without which this work would not have been completed. The National Science Foundation provided computing time on the CRAY X-MP at the National Center for Supercomputing Applications.

REFERENCES

Aikawa, T. & Simon, N. R., 1983. *Astrophys. J.*, **273,** 346.
Clement, C. M., Nemec, J. M., Robert, N., Wells, T., Dickens, R. J. & Bingham, E. A., 1986. *Astr. J.*, **92,** 825.
Cox, A. N., 1988. In: *Second Conference on Faint Blue Stars,* p. 161, eds Philip, A. G. D., Hayes, D. S. & Liebert, J. W., L. Davis Press, Schenectady.
Cox, A. N., Hodson, S. W. & Clancy, S. P., 1983. *Astrophys. J.*, **266,** 94.
Hubickyj, O. & Stothers, R. B., 1986. *Astrophys. J.*, **309,** 122.
Kovacs, G., 1990. In: *The Numerical Modelling of Nonlinear Stellar Pulsations; Problems and Prospects,* ed. Buchler, J. R., Reidel, Dordrecht, in press.
Kovacs, G. & Buchler, J. R., 1988. *Astrophys. J.*, **324,** 1026.
Lub, J., 1977. *Astr. Astrophys. Suppl.*, **29,** 345.
Petersen, J. O., 1984. *Astr. Astrophys.*, **139,** 496.
Rood, R. T. & Crocker, D. A., 1989. In: *The Use of Pulsating Stars in Fundamental Problems of Astronomy,* p. 103, ed. Schmidt, E. G., Cambridge University Press, Cambridge.
Simon, N. R., 1984. *Astrophys. J.*, **284,** 278.
Simon, N. R., 1985. *Astrophys. J.*, **299,** 723.
Simon, N. R., 1988a. In: *Pulsation and Mass Loss in Stars,* p. 27, eds Stalio, R. & Willson, L. A., Reidel, Dordrecht.
Simon, N. R., 1988b. *Astrophys. J.*, **328,** 747.
Simon, N. R., 1989. *Astrophys. J.*, **343,** L17 (S89).
Simon, N. R. & Aikawa, T., 1986. *Astrophys. J.*, **304,** 249.
Simon, N. R. & Lee, A. S., 1981. *Astrophys. J.*, **248,** 291.
Stellingwerf, R. F., 1975. *Astrophys. J.*, **195,** 441.
Stothers, R. B., 1981. *Astrophys. J.*, **247,** 941.
Uje-iye, K. I., 1986. *Science Reports of the Tohoku University, Series 98,* **6,** 173.
Ulrich, T. G. & Bishop, T. N., 1975. *Rev. Geophys. Space Phys.*, **13,** 183.